Molecular basis for the stability relationships between homochiral and racemic crystals of tazofelone: a spectroscopic, crystallographic, and thermodynamic investigation

Susan M. Reutzel-Edens,* Victoria A. Russell and Lian Yu

Lilly Research Laboratories, Eli Lilly and Company, Indianapolis, IN 46285, USA

Received (in Cambridge, UK) 23rd November 1999, Accepted 4th February 2000

Tazofelone (**1**) has been crystallized as two polymorphic racemic compounds (**1a**), designated **I** and **II**, and as an (*S*)-(−) enantiomorph (**1b**). These crystal forms have been characterized using FTIR and solid-state NMR spectroscopy, single crystal X-ray analysis, and differential scanning calorimetry. The stability relationship of the racemic polymorphs has been established as enantiotropic, with form **II** being low-temperature stable and form **I** being high-temperature stable (transition temperature 138 °C). These two forms have similar enthalpies, entropies, and free energies (thermodynamic stability), which may be related to their similar molecular conformations, hydrogen-bonding patterns, and crystal packing efficiencies. The racemic crystals are significantly more stable than the physical mixture of the enantiomorphs. The spontaneous conversion of the racemic crystals into the conglomerate is not feasible thermodynamically at any temperature (monotropy). The weak lattice of the enantiomorphs may result, in part, from the high energy conformers that are the building blocks of the enantiomorphs and weaker dipole–dipole interactions.

Introduction

Organic molecules pack in crystal structures that represent an energetic balance between molecular structure, conformation, and intermolecular forces (van der Waals, dipolar, hydrogen bonding, *etc.*), as well as a thermodynamic compromise between tendencies toward low energy and high entropy. Considerable effort has gone into understanding the interplay of the intermolecular forces among classes of compounds, leading to novel approaches to crystal engineering.[1] Polymorphism, considered a nemesis to many in the field of crystal engineering, provides a unique opportunity to study the influence of crystal forces on molecular conformation[2] and the balance between intramolecular and intermolecular interactions in molecular solids.[3]

The crystallization of chiral molecules gives rise to a special kind of "polymorphism": enantiomorphs are constructed of molecules of the same chirality and racemic compounds contain molecules of opposite chirality in the same unit cell.[4] Enantiomers and racemates, while not true polymorphs of one another,[5] are logical candidates for extending studies on polymorphism. For these systems, the influence of enantiomeric interactions on conformation and crystal packing forces (van der Waals, electrostatic, hydrogen bonding) must also be considered. While considerable attention has been given to determining the biological (pharmacological and toxicological) effects of chirality,[6] comparatively few studies have been directed toward understanding fundamental aspects of enantiomeric interactions (or favorable packing arrangements in racemic space groups) in the solid state and their effects on physicochemical properties.[7] These studies are especially important for the resolution of enantiomers in cases where a therapeutic benefit to administering a single enantiomer is observed.[8]

Tazofelone (5-[(3,5-di-*tert*-butyl-4-hydroxyphenyl)methyl]-1,3-thiazolidin-4-one) (**1**) is a potent antioxidant and 5-lipoxygenase inhibitor recently investigated as a novel therapy for inflammatory bowel diseases (IBD): colitis, proctitis, and Crohn's disease.[9] The molecule, which possesses one chiral center, has been isolated as a racemic mixture of *R* and *S* enantiomers, **1a**, and as the pure enantiomers (**1b** = *S*, **1c** = *R*).

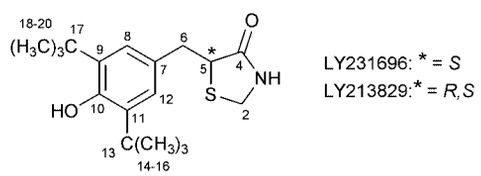

(*R*,*S*)-Tazofelone (**1a**) has been crystallized as two polymorphic racemic compounds, **I** and **II**. Crystallization of racemic solutions of tazofelone often resulted in mixtures of **I** and **II**. When the pure *S* (or *R*) enantiomer was crystallized, an altogether different crystal form was isolated. The enantiomorph crystal form (**1b** or **1c**) has never been isolated from racemic solutions. To understand the structural and thermodynamic basis for this behavior, the crystal forms of tazofelone were characterized by crystallographic, spectroscopic, and thermal methods.

Experimental

Materials

(*R*,*S*)-Tazofelone was synthesized at the Lilly Research Laboratories (Indianapolis, IN).[10] The pure enantiomers [**1b**: (*S*)-(−), LY231696, **1c**: (*R*)-(+), LY231697] were isolated by separating diastereomeric thiazolidinone precursors, followed by chemoselective benzylamide cleavage,[11] or directly separated by a kinetic resolution involving enantioselective sulfoxide formation.[12]

For the spectroscopic and thermal analyses, samples of **1a** (form **I**) were crystallized from ethyl acetate; **1a** (form **II**) was prepared by slurrying form **I** in a 1:1 mixture of ethyl acetate and heptane at 25 °C; **1b** was crystallized from 5:1 hexanes–EtOAc. For the single crystal X-ray analyses, colorless plates of form **I** were crystallized from toluene; colorless prisms/rods of form **II** were crystallized by slow evaporation from acetonitrile at 25 °C; pale yellow prisms and thick hexagonal-shaped plates

DOI: 10.1039/a909259e

Table 1 Crystal data and structure refinement parameters

	1a (I)	1a (II)	1b
Formula	$C_{18}H_{27}NO_2S$	$C_{18}H_{27}NO_2S$	$C_{18}H_{27}NO_2S$
FW	321.47	321.47	321.47
Space group	$P2_1/c$ (#14)	$Pbca$ (#61)	$P2_1$ (#4)
Crystal system	Monoclinic	Orthorhombic	Monoclinic
a/Å	11.313(3)	17.204(3)	9.392(2)
b/Å	17.082(4)	11.287(3)	10.962(2)
c/Å	19.324(7)	18.860(7)	17.823(4)
β/°	101.11(2)	90	94.29(3)
V/Å^3	3665(2)	3662.2(2)	1829.8(6)
Z	8	8	4
ρ_{calc}/g cm^{-3}	1.165	1.166	1.167
T/K	293	295	293
Scan mode	ω	2θ–θ	ω
2θ range, radiation	7–114, Cu	0–116, Cu	5–114, Cu
Range of hkl	+12, +18, −21/20	+18, +12, −20	+10, +11, ±19
Reflections collected	5221	2847	2802
Unique reflections	4928	2496	2620
R_{int} (%)	4.78	0.00	2.82
Observed reflections	4914 ($I > 2\sigma(I)$)	2167 ($I > 4\sigma(I)$)	2617 ($I > 2\sigma(I)$)
Corrections applied[a]	none	2	1,[b] 2
Parameters	399	200	422
$R(F)$	0.0636	0.0494	0.0554
$R_w(F)$[c]	0.1911	0.095	0.1413
GOF	1.144	2.66	0.941
$\Delta(\rho)$/e$^-$ Å^{-3}	0.31	0.39	0.42
Extinction coefficient	1.7×10^{-4}	5.2×10^{-3}	0.3×10^{-3}

[a] 1 = Empirical absorption, 2 = secondary extinction, **1a (II)**: $F^* = F[1 + 0.002\chi F^2/\sin(2\theta)]^{-1/4}$ **1b**: $F_c^* = F[1 + 0.001\chi F_c^2\lambda^3/\sin(2\theta)]^{-1/4}$. [b] Semi-empirical absorption correction; $\mu = 1.615$. [c] **1a (I)**: $w^{-1} = [\sigma^2(F_o^2) + (0.1164P)^2 + 1.9481P]$, where $P = (F_o^2 + 2F_c^2)/3$; **1a (II)**: $w^{-1} = \sigma^2(F) + 0.0004F^2$; **1b**: $w^{-1} = [\sigma^2(F_o^2) + (0.0824P)^2 + 1.9985P]$, where $P = (F_o^2 + 2F_c^2)/3$.

of the enantiomorph were crystallized by slow evaporation from methanol at 25 °C.

Differential scanning calorimetry (DSC)

DSC was conducted using a Seiko DSC 210 under 50 mL min^{-1} N_2 purge at a heating rate of 10 °C min^{-1} for samples in crimped aluminum pans. The temperature and heat flow were calibrated using indium. The melting and eutectic melting data reported in the text were the average of 2–3 measurements. The melting temperatures were the onsets of melting endotherms. Standard errors were approximately ±0.05 °C for temperatures and ±0.1 kJ mol^{-1} for heats.

Infrared spectroscopy

Diffuse reflectance FTIR spectra were obtained on a Mattson Galaxy 5020 spectrometer, equipped with a deuterated triglycine sulfate (DTGS) detector and Spectra-Tech Baseline™ diffuse reflectance accessory and operated under a dry air purge. Typical measurement conditions were as follows: 100 co-added background and sample scans collected at 4 cm^{-1} resolution with a spectrometer gain of 1. Spectra were ratioed to the background spectrum of dry FTIR-grade KBr.

Solid-state NMR spectroscopy

^{13}C Cross polarization/magic angle spinning (CP/MAS) NMR spectra were obtained using a Varian Unity 400 MHz spectrometer operating at a carbon frequency of 100.577 MHz and equipped with a complete solids accessory and Varian 7 mm VT CP/MAS probe. Typical measurement conditions were as follows: 90° proton rf pulse 4 μs, contact time 1 ms, pulse repetition time 5 s, MAS frequency 7 kHz, spectral width 50 kHz, and acquisition time 50 ms. The chemical shifts were referenced to the CH_3 of hexamethylbenzene ($\delta = 17.3$ ppm) by sample replacement. Interrupted decoupling spectra were obtained with a 50 μs delay without decoupling prior to acquisition.

^{15}N CP/MAS NMR spectra were obtained at a nitrogen frequency of 40.538 MHz using a Varian 7 mm VT CP/MAS probe. Hartmann–Hahn match parameters were determined using glycine–^{15}N. Measurement conditions were as follows: 90° proton rf pulse 7 μs, contact time 2.5 ms, relaxation delay 5 s, acquisition time 0.1 s, MAS speed 3.0 kHz, and spectral width 35 kHz. Chemical shifts were externally referenced to $^{15}NH_4Cl$ using sample replacement.[13]

Crystal structure determinations

X-Ray crystal data were collected on a Siemens R3m/V diffractometer with graphite monochromated Cu-Kα radiation ($\lambda = 1.54178$ Å). Data reduction was performed with SHELXTL-PLUS[14] and structures solved with direct methods using SHELX-86.[15] The **1a** (form **I**) and **1b** structures were refined using SHELXL-93.[16] The **1a** (form **II**) structure was refined using SHELX-86. All non-hydrogen atoms were refined anisotropically. Methyl hydrogen atom positions, R–CH_3, were optimized by rotation about R–C bonds with idealized C–H, R–H, and H–H distances. The remaining hydrogen atoms were included in the structure factor calculations as fixed idealized contributors, with assigned isotropic thermal parameters ($B = 1.2 \times B_{eq}$ of bonded atoms). The hydrogen attached to the chiral carbon in the enantiomorph was refined in order to assign absolute configuration. Using the Cerius2 crystal modeling program,[17] the phenol hydrogens were placed in locations consistent with hydrogen bonding to neighboring amide carbonyl acceptors for illustration purposes. Experimental details of the structure determinations are given in Table 1. CCDC number 188/229. See http://www.rsc.org/suppdata/p2/a9/a909259e for crystallographic files in .cif format.

Crystallographic literature search

A connectivity search of the Cambridge Crystallographic Database (Version 5.14)[18] was performed for 2,6-di-*tert*-butylphenols. A total of 27 unique structures were retrieved. A search for the amide···phenol six-membered ring hydrogen-bonding motif was also conducted. A total of 20 structures were retrieved featuring both an amide (O=C–N–H) and a phenol (Ph–O–H).

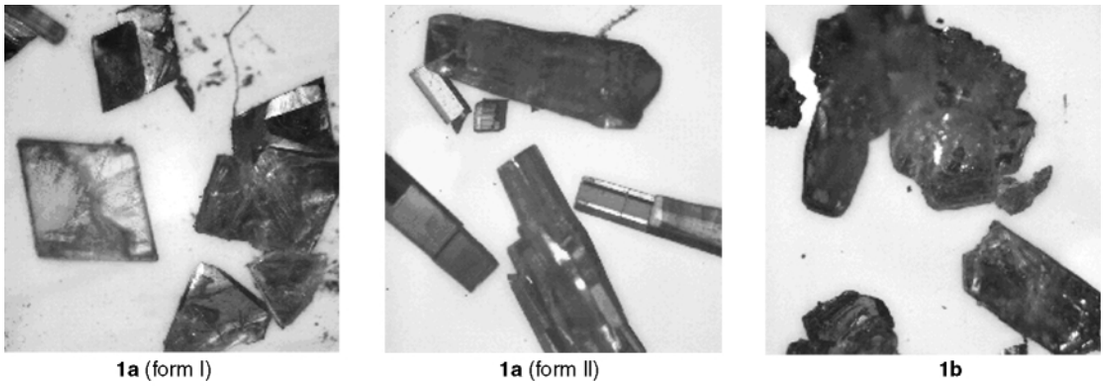

Fig. 1 Distinct crystal morphologies of polymorphic tazofelone racemates, **1a** (forms **I** and **II**), and enantiomorph, **1b**.

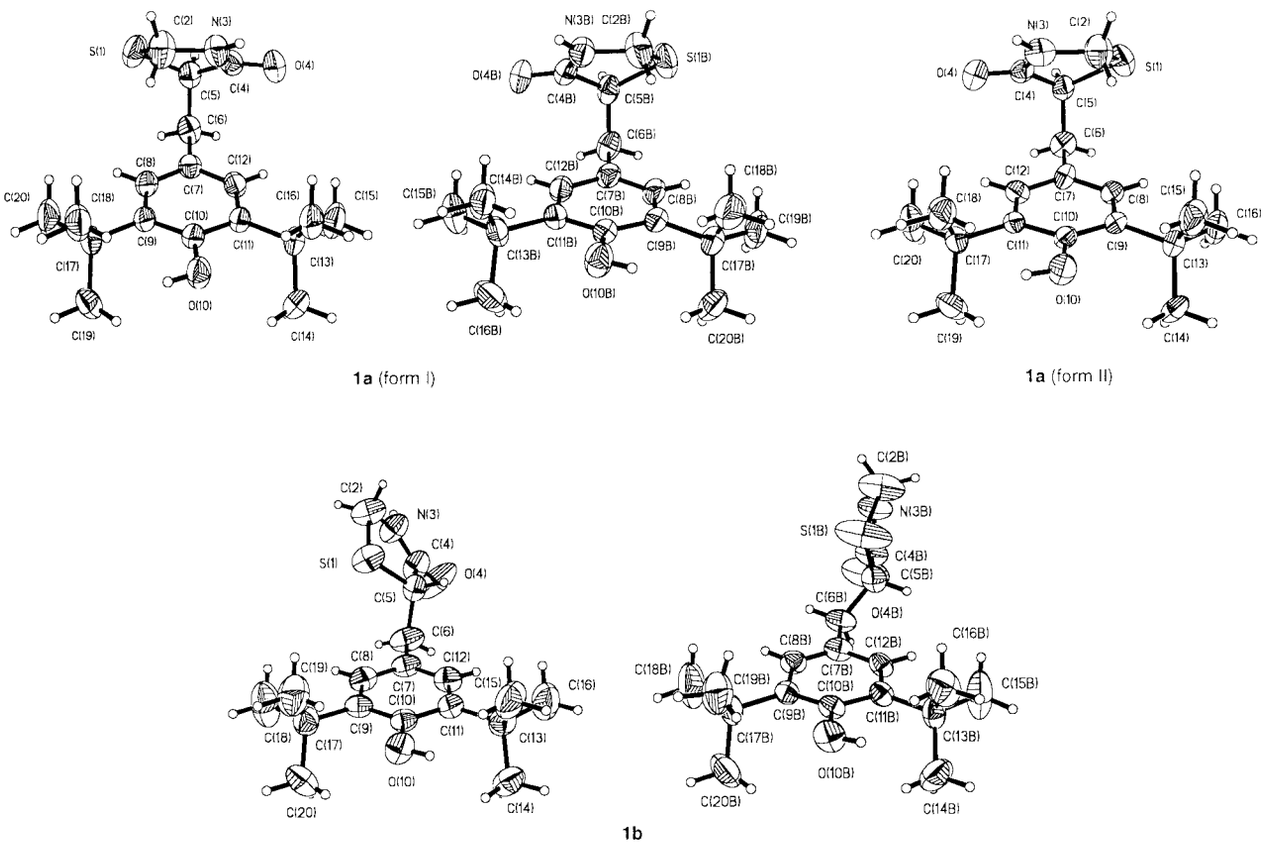

Fig. 2 ORTEP drawings (50% probability ellipsoids) of asymmetric units and atomic numbering schemes.

Computational details

Ab initio methods were employed to calculate the conformational energies and to conduct a conformer search. The commercial program Spartan (Version 5.0) was used.[19] The conformational energies of different crystal conformers were compared using "H-corrected" structures, which were generated by freezing all non-hydrogen atoms and the hydroxy orientation relative to the phenyl ring and minimizing the geometry. The conformer search began with the conformer in **1a** (form **II**) and involved systematically varying the two exocyclic torsion angles (S1–C5–C6–C7 and C5–C6–C7–C8) which define the molecular shape of **1** in increments of 120° (a 3 × 3 matrix) and optimizing the resulting geometry (RHF/3-21G(*)). Lattice energy calculations were performed using the X-ray structure data (coordinates, unit cell dimensions, space group) and atomic charges (obtained by *ab initio* calculations for each conformer) as input to the Cerius[2] program. The crystal structures were optimized (total energy was minimized) using DREIDING,[20] CFF,[21] and consistent-valence (CVFF)[22] forcefields and the lattice energies calculated.

Results

Recrystallization of **1a** yielded two polymorphic forms (**I** and **II**), with frequent observation of mixtures of the two crystal phases. A different crystal form of tazofelone was isolated by crystallizing a pure sample of **1b**. These crystal forms were easily differentiated by their unique morphologies (Fig. 1) and by X-ray powder diffraction and solid-state ^{13}C NMR spectroscopy. Crystal structures of **1a** (forms **I** and **II**) and **1b** were solved, permitting a detailed evaluation of the structure and bonding responsible for racemate formation, polymorphism, physical stability, and crystal morphology. ORTEP views of the asymmetric units and atomic labeling are given in Fig. 2.

Molecular structure and conformations

Racemate **1a** adopts virtually superimposable, "folded" conformations in forms **I** and **II** (Fig. 2). Whereas the *R* and *S* enantiomers are nearly inversion-related in form **I**, they are related by true crystallographic inversion symmetry in form **II**. Two molecules are present in the asymmetric unit of **1b**, each

Table 2 Selected bond lengths (Å) and torsion angles (°)

Site (D–H · · · A)	1a (I)	1a (II)	1b
C(4)–O(4)	1.237	1.243	1.203
C(4B)–O(4B)	1.237		1.230
S(1)–C(5)–C(6)–C(7)	−67.7	68.6	−62.6
S(1B)–C(5B)–C(6B)–C(7B)	67.7		−55.9
C(5)–C(6)–C(7)–C(8)	88.2	−88.9	−82.0
C(5B)–C(6B)–C(7B)–C(8B)	−91.0		132.3

adopting an "extended" conformation, but differing significantly in the relative orientation of their lactam and phenol rings. Torsion angles describing the molecular conformations are listed in Table 2.

Hydrogen bonding

Hydrogen bonding plays a key role in determining crystal packing in **1**. The molecule features two hydrogen-bond donors, the amide NH and phenol OH, and two acceptors, the lactam carbonyl (which is capable of accepting two hydrogen bonds) and phenol oxygens. Each donor and acceptor site, except the phenol hydroxy oxygen acceptor, participates in hydrogen bonding in **1a** (forms **I** and **II**). The basic molecular building block in both racemic polymorphs is an eight-membered ring N–H · · · O hydrogen-bonded amide dimer of graph set R_2^2 (8) formed between opposite enantiomers.[23]

While the two inversion-related enantiomers form a centrosymmetric dimer in form **II**, the crystallographically inequivalent enantiomers that dimerize in polymorph **I** are related by pseudo-inversion symmetry. Interestingly, the dimers in **I** and **II** are virtually superimposable, suggesting that crystallographic inequivalence observed in **I** is a consequence of packing the building blocks in three-dimensional space.

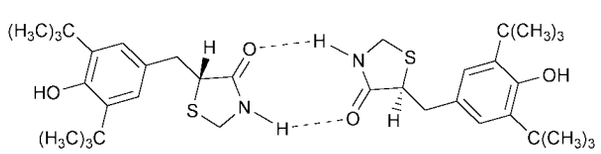

1a

The phenol hydrogen in **1** is significantly sterically hindered by the *ortho*-Bu^t groups and might not be expected *a priori* to participate in hydrogen bonding. Adjacent molecules are clearly aligned with the phenol and lactam carbonyl oxygens in close proximity in forms **I** and **II**, suggesting that the hindered phenol OH groups are indeed directing molecular aggregation. The O · · · O distances are relatively long (2.903 and 2.897 Å in **I**; 2.898 Å in **II**), but still fall within accepted van der Waals distance criterion for a hydrogen bond.[24] The geometry of the O–H · · · O hydrogen bonds appears to be less than optimal, however, the angle criterion is generally less stringent.[25]

A Cambridge Structural Database search was conducted to discern whether similar interactions have been observed in the structures containing phenol hydroxy groups hindered on both sides by Bu^t groups. Hydrogen-bonding interactions were observed in five of the 27 di-*tert*-butylphenol structures ($d_{O\cdots O(cutoff)}$ = 3.0 Å), two of which involve hydrogen bonds to amide carbonyl oxygens (JOWTIY and VOGMAF).[26]

Hydrogen-bonding distances for the crystal forms of **1** are summarized in Table 3.

The O–H · · · O hydrogen bonds between the phenol hydroxy groups and the *anti* amide carbonyl lone electron pair acceptors in **I** and **II** link adjacent screw-related amide dimers into virtually-identical two-dimensional hydrogen-bonded layers (Fig. 3). The hydrogen-bonded layers are parallel to the (001) plane in both polymorphs. The alignment of the hydrogen-bonded layers in the *ab* planes is evident from the respective unit cell parameters (form **I**, a = 11.31 Å, b = 17.08 Å; form **II**, b = 11.29 Å, a = 17.20 Å).

Table 3 Hydrogen-bonding distances and geometries

Site	$d_{D\cdots A}$/Å	Symmetry relation of A
1a (I)		
N(3)–H · · · O(4B)	2.880	x, y, z
N(3B)–H · · · O(4)	2.890	x, y, z
O(10B)–H · · · O(4B)	2.903	$-x, y + 1/2, -z + 1/2$
O(10)–H · · · O(4)	2.897	$-x, y + 1/2, -z + 1/2$
1a (II)		
N(3)–H · · · O(4)	2.891	$-x, -y, -z$
O(10)–H · · · O(4)	2.898	$x + 1/2, -y + 1/2, -z$
1b		
N(3)–H · · · O(10)	2.943	$x, y + 1, z$
O(10)–H · · · O(5)	2.812	$x, y + 1, z$
N(3B)–H · · · O(10B)	2.917	$x, y + 1, z$
O(10B)–H · · · O(5B)	2.651	$x, y + 1, z$

The hydrogen-bonding interactions observed in **1b** are significantly different from those in the racemic polymorphs. Rather than forming two-dimensional hydrogen-bonded layers [as observed in **1a** (forms **I** and **II**)], translationally-related molecules are linked into chains by hydrogen bonds between the amide and phenol, Fig. 3. The higher energy, extended molecular conformation (see later) presumably enables the amide and sterically-hindered phenol to form a six-membered ring motif of graph set R_2^2 (6). In this motif, the hydroxy group acts as a donor ($d_{O-H\cdots O}$ = 2.651 and 2.812 Å) and an acceptor ($d_{O\cdots H-N}$ = 2.943 and 2.917 Å) to the amide group. A search of the Cambridge Structural Database revealed that the amide · · · phenol ring motif is extremely rare. None of the 20 structures that contained both an amide (C(O)–NH) and a phenol (Ar–OH) featured this motif.

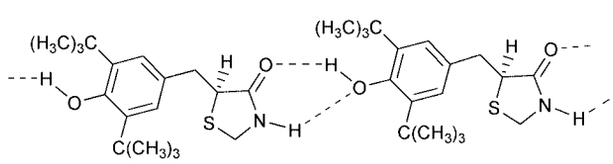

1b

Crystal packing

The packing of the hydrogen-bonded layers in **1a** (form **I**) likely causes the symmetry of the amide dimer to be reduced from that of **1a** (form **II**). Because forms **I** and **II** crystallize in different space groups ($P2_1/c$ and $Pbca$, respectively), the two-dimensional hydrogen bonded layers stack differently (Fig. 4), effectively changing the symmetry relationship between them. In **I**, the hydrogen-bonded layers are screw-related, whereas in **II**, the layers are glide-related. Interestingly, the density (and packing coefficient,[27] κ) is comparable in the polymorphic racemates (**I**: ρ = 1.165 g cm^{-3}, κ = 0.72; **II**: ρ = 1.166 g cm^{-3}, κ = 0.73).[28] The considerable similarity between the molecular conformation, hydrogen bonding, and packing efficiency in **1a** (forms **I** and **II**) may explain their similar properties and frequent co-precipitation. The different crystal packing, on the other hand, results in notably distinct crystal morphologies observed for the racemic polymorphs (Fig. 1).

In contrast to **1a** (forms **I** and **II**) that features close-packed two-dimensional hydrogen-bonded layers, the **1b** structure is a product of the close packing of one-dimensional chains. In this structure, translationally-related molecules linked by the head-to-tail bidentate amide · · · phenol hydrogen bonds form

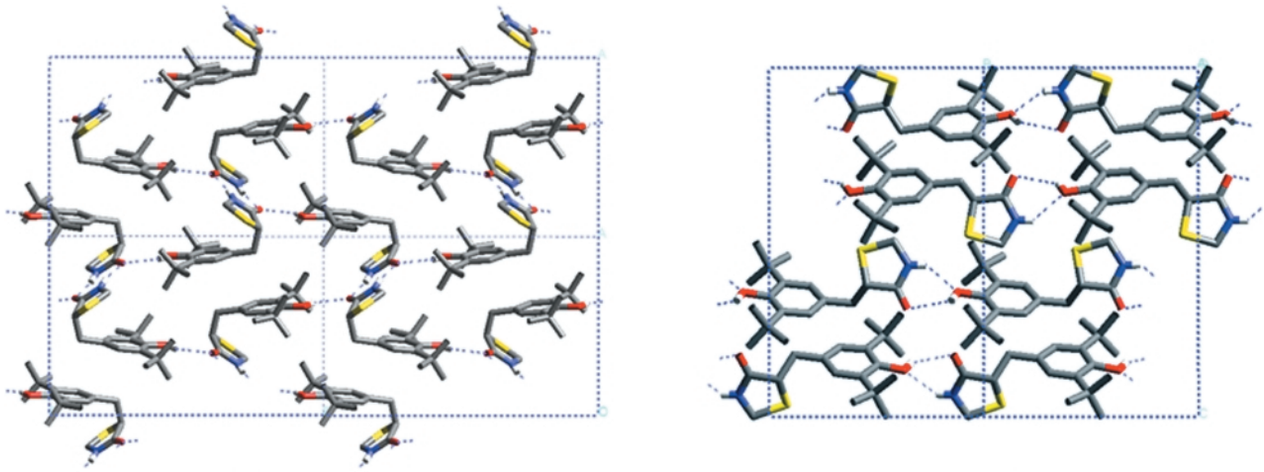

Fig. 3 Hydrogen-bonded layers in **1a** (forms **I** and **II**) and hydrogen-bonded chains in **1b**. The C–H hydrogen atoms have been omitted for clarity.

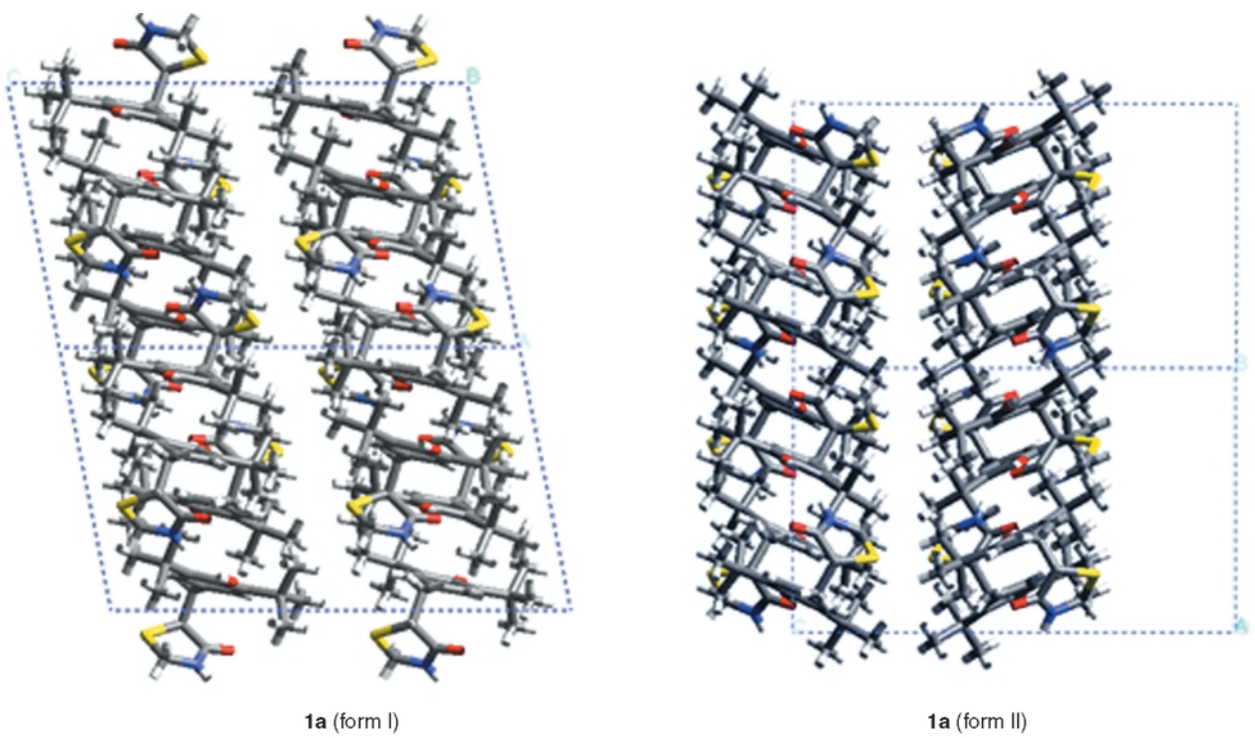

Fig. 4 Three-dimensional packing of hydrogen-bonded layers in **1a** (forms **I** and **II**).

discrete chains parallel to the *y*-axis. Two pseudo-inversion-related chains are formed by the crystallographically-distinct molecules (Fig. 3). Symmetry-related chains in the crystal are then generated by the 2_1-screw operation applied to the two unique chains. Despite the impossibility of molecular packing *via* inversion centers, which often leads to greater packing efficiency,[29] the hydrogen-bonded chains pack as efficiently ($\rho = 1.167$ g cm^{-3}, $\kappa = 0.73$) as the two-dimensional layers in the polymorphic racemates.

Solid-state spectroscopy

Solid-state spectroscopy, which has previously been shown to be a powerful tool for studying structure and bonding (both intra- and intermolecular) in organic solids,[30] was particularly useful for characterizing the tazofelone crystal forms. FTIR spectra collected for the racemic polymorphs and pure enantiomorph clearly reveal similarities (and differences) in these crystal structures (Fig. 5). For example, the virtually identical molecular conformations and intermolecular interactions in **1a** (forms **I** and **II**) are reflected in their nearly superimposible FTIR spectra. In both spectra, the amide carbonyl stretching bands appear at 1675 cm^{-1} and slightly broadened OH stretches, suggestive of weak hydrogen bonding, are observed at 3560 cm^{-1}. Interestingly, the different crystal packing observed in these structures has relatively little effect on the FTIR spectra. A slight splitting of the aromatic C⋯C stretch at 1380–1400 cm^{-1} and the broadening of the carbonyl stretch at 1675 cm^{-1} in form **I** may reflect the two crystallographically-inequivalent molecules in this crystal form.

The unique hydrogen-bonding pattern observed in **1b** is obvious from the FTIR spectra. Shifting of the OH, NH, and C=O stretches reflects the different strengths of the hydrogen-bonding interactions to the amide and phenol functional groups. Specifically, the OH stretching band of **1b** is red-shifted and broadened (**1b**: 3495 cm^{-1}; **1a** (forms **I** and **II**): 3555–3560 cm^{-1}), which is consistent with a stronger OH⋯O hydrogen bond in this crystal form. The NH and C=O stretches, on the other hand, are observed at higher frequencies (**1b**: 3350 and 1695 cm^{-1}, respectively; **1a** (forms **I** and **II**): 3170 and 1675

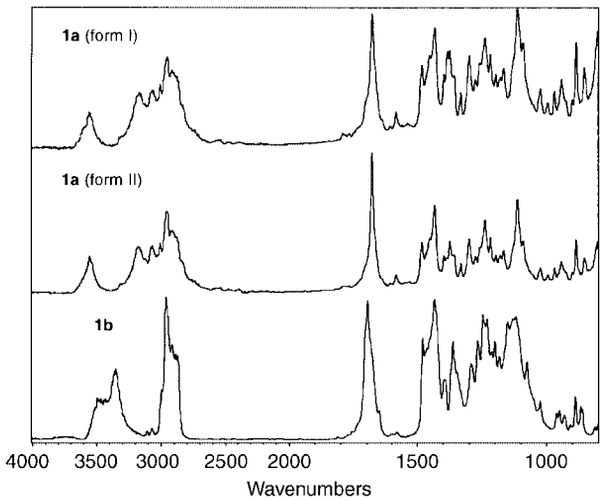

Fig. 5 Diffuse reflectance FTIR spectra of **1a** (forms **I** and **II**) and **1b**.

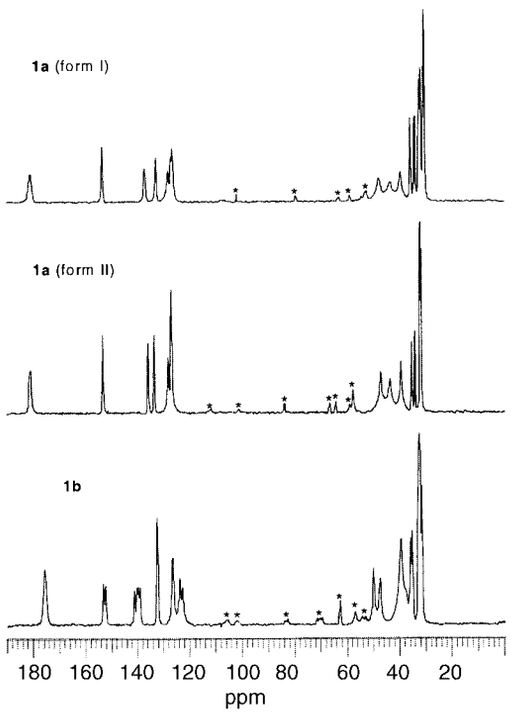

Fig. 6 ^{13}C CP/MAS NMR spectra of **1a** (forms **I** and **II**) and **1b**. Spinning sidebands are denoted by asterisks (*).

cm^{-1}, respectively) consistent with the weaker hydrogen bonding to the lactam in **1b**.

Whereas the FTIR spectra of **1a** (forms **I** and **II**) are nearly identical, ^{13}C SSNMR spectra of all of the crystal forms of **1** are unique (Fig. 6). The spectra feature resonances of somewhat variable linewidth, which can be attributed to different decoupling efficiency (methylene peaks at 25–50 ppm are comparatively broad), dipolar coupling to quadrupolar ^{14}N (lactam carbonyl peaks are somewhat broad),[31] and/or overlapping resonances. Considering these sources of line broadening, a high degree of crystallinity is apparent from the sharp ^{13}C peaks in each spectrum.

Despite the lower resolution inherent in solid-state NMR spectroscopy, many more resonances are observed in the ^{13}C SSNMR spectrum of **1** than in the solution state (spectrum not shown), where rapid molecular motion renders the halves of the di-*tert*-butylphenol ring equivalent. The peak multiplicity in the SSNMR spectrum is due in part to severely restricted molecular motion in the solid state, which causes resonances of the nominally equivalent carbons of the di-*tert*-butylphenyl ring to split. A slight splitting of the carbonyl resonance near 180 ppm is also observed in **II**, due to dipolar coupling to the adjacent quadrupolar ^{14}N. Since only one molecule was identified in the asymmetric unit of **1a** (form **II**), additional peak splitting would not be expected in the SSNMR spectrum of this crystal form. Not surprisingly, only one peak is observed for each carbon nucleus in its SSNMR spectrum. Form **I** also appears to have a single molecule in the asymmetric unit, however, upon close inspection (with the aid of resolution enhancement), additional splitting is seen for the C(9) (and C(11)) resonance near 137 ppm in its SSNMR spectrum. This splitting is consistent with two crystallographically-inequivalent molecules. Unlike form **I**, two molecules are readily identified in the asymmetric unit of **1b** by peak doubling across its SSNMR spectrum.

^{13}C CP/MAS spectral assignments were made by comparing chemical shifts observed in completely decoupled solution and dipolar dephased ^{13}C NMR spectra.[32] Chemical shifts observed in the solution and solid-state NMR spectra are sufficiently close, as expected since no changes in molecular structure accompany the crystallization of the solid forms of **1**. Chemical shift differences may therefore be interpreted in terms of molecular conformation, hydrogen-bonding interactions, and/or crystal packing preferences. For example, the significantly different lactam C(5) and C(5B) chemical shifts in **1b** can be attributed to conformational differences, which place these carbons in significantly different environments. Specifically, C(5B) is positioned in a less shielded region of the phenol ring than is C(5) in **1b** (or C(5)/C(5B) in **1a**), causing its resonance to be shifted 2–3 ppm downfield. Other chemical shift differences between non-hydrogen-bonding centers are likely induced by crystal packing preferences. The C(9) and C(11) resonances are considerably shifted with respect to one another in **1a** (forms **I** and **II**), a difference which has proven to be useful for quantifying the crystal phase purity of racemic mixtures. Most of the chemical shifts observed in solution are intermediate of those observed in the solid state, which suggests that a conformationally-averaged structure is present in solution.

The chemical shifts of highly anisotropic carbonyl carbons are particularly sensitive to changes in solid-state electronic environments induced by hydrogen-bonding interactions. The carbonyl carbon resonances of **1a** (forms **I** and **II**), for example, are significantly downfield-shifted (~5 ppm) in each SSNMR spectrum relative to **1b** as expected due to the stronger hydrogen bonding in the racemic polymorphs. The solution-state carbonyl carbon chemical shift is intermediate of those observed for the racemic compound and enantiomorph crystals, suggesting that tazofelone also aggregates in solution. Chemical shift data and peak assignments are summarized in Table 4.

^{15}N CP/MAS NMR spectroscopy was also used to characterize the hydrogen-bonding interactions to the NH donor in the racemic and enantiomorph crystal forms. Single amide nitrogen resonances are observed in each ^{15}N SSNMR spectrum (Fig. 7). Peak doubling is not observed in either **1a** (form **I**) or **1b**, presumably because of insufficient resolution of substantially-dipolar broadened amide ^{15}N resonances.

Depending on whether a nitrogen atom participates in hydrogen bonding as an acceptor or donor, its ^{15}N resonance will shift to higher or lower frequencies, respectively.[33] Since the amide is expected to behave solely as a hydrogen-bond donor, its ^{15}N resonance is expected to shift downfield as this center participates in hydrogen bonding, the extent to which will be commensurate with the type and strength of the interaction. Indeed, the ^{15}N resonances in forms **I** and **II** are shifted downfield (by 11 and 12 ppm, respectively) from that of **1b**, confirming that the amide NH group in **1a** (forms **I** and **II**) is more strongly hydrogen-bonded to the carbonyl acceptors than in **1b**.

Stability relationship between racemic polymorphs

Because mixtures of forms **I** and **II** were frequently observed, determining their relative stability was particularly important for controlling polymorph selectivity throughout the crystallization process of **1a**. The stability relationship between the structurally similar forms **I** and **II** could be qualitatively determined from their melting and eutectic melting data. The higher melting point of Form **I** (Table 5) indicates that **I** is more stable than **II** near the melting region. The lower heat of fusion of the higher melting **I** (37.8 kJ mol^{-1} in **I** *vs.* 39.2 kJ mol^{-1} in **II**) indicates that the crystal forms are enantiotropic (Heat of Fusion Rule).[34] The enantiotropic relationship between the two racemic polymorphs (**I** and **II**) is also evident from their eutectic melting data (Table 5). Whereas form **I** is the higher melting and more stable form near the melting region, form **II** has higher eutectic melting temperatures below 134 °C, indicating that form **II** is low-temperature stable.

To quantify the stability relationship between forms **I** and **II**, the free energy difference, ΔG, between the true polymorphs has been determined as a function of temperature using melting[35] [eqns. (1) and (2)] and eutectic melting[36] [eqns. (3) and (4)] data as follows:

$$(G_{RI} - G_{RII})(T_{mI}) = \Delta H_{mII}(T_{mII} - T_{mI})/T_{mII} \quad (1)$$

$$(G_{RI} - G_{RII})(T_{mII}) = \Delta H_{mI}(T_{mII} - T_{mI})/T_{mI} \quad (2)$$

$$(G_{RI} - G_{RII})(T_{eI}) = \Delta H_{meII}(T_{eII} - T_{eI})/(x_{eII}T_{eII}) \quad (3)$$

$$(G_{RI} - G_{RII})(T_{eII}) = \Delta H_{meI}(T_{eII} - T_{eI})/(x_{eI}T_{eI}) \quad (4)$$

Here G_{RI} and G_{RII} are the free energies, T_{mI} and T_{mII} are the melting points of racemic compounds **I** and **II**, T_{eI} and T_{eII} are the eutectic melting temperatures with common reference compounds (RC), x_{eI} and x_{eII} are the eutectic compositions, and ΔH_{mI}, ΔH_{mII}, ΔH_{meI}, and ΔH_{meII} are the heats of melting.[37]

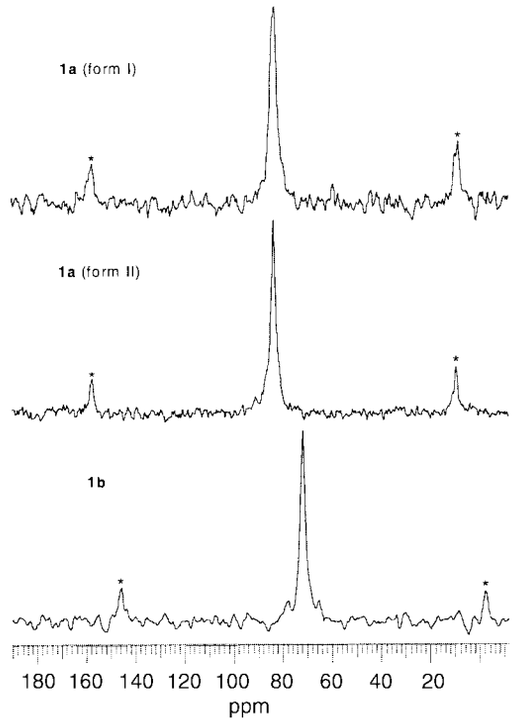

Fig. 7 ^{15}N CP/MAS NMR spectra of **1a** (forms **I** and **II**) and **1b**. Spinning sidebands are denoted by asterisks (*).

The ΔG *vs.* T plot (Fig. 8), which is referenced to form **II** by convention, reveals a rather small free energy difference between the racemic polymorphs of **1**. The enantiotropic

Table 4 Solution ($CDCl_3$) and/or solid-state ^{13}C and ^{15}N NMR chemical shift data for tazofelone (ppm)

Site	Solution	**1a (I)**	**1a (II)**	**1b**
C(2)	41.14	43.3	43.8	39.6
C(4)	177.74	181.0[a]	180.9,[a] 181.4[a]	175.7[a]
C(5)	48.90	47.7	47.2	46.7, 50.0
C(6)	39.59	39.4	39.4	39.6
C(7)	128.23	126.8[a]	127.0[a]	132.4[a]
C(8), C(12)	125.69	126.3, 128.0	127.0, 128.1	122.8, 123.9, 126.5
C(9), C(11)	135.78	132.7,[a] 136.8[a]	133.5,[a] 135.8[a]	139.1,[a] 139.8,[a] 140.3,[a] 141.2[a]
C(10)	152.65	153.3[a]	153.2[a]	152.3,[a] 153.1[a]
C(13), C(17)	34.22	33.8,[a] 35.5[a]	34.2,[a] 35.3[a]	35.3, 35.9
C(14)–C(16), C(18)–C(20)	30.26	30.4,[a] 31.6,[a] 32.4[a]	31.7,[a] 32.2[a]	31.6, 32.5
N(3)	—	82.2	83.8	71.9

[a] Chemical shifts observed in interrupted decoupling spectra.

Table 5 Melting and eutectic melting data of the tazofelone crystal forms[a]

Reference compound	**1a (I)**			**1a (II)**		
	χ_e	T_m or T_e/°C	ΔH_m/kJ mol^{-1}	χ_e	T_m or T_e/°C	ΔH_m/kJ mol^{-1}
None	—	156.6	37.8	—	154.7	39.2
Benzanilide	0.51	133.4	33.9	0.52	133.8	33.3
p-Acetophenetidide	0.33	119.8	32.5	0.33	120.3	32.3
Acetanilide	0.19	101.6	21.9	0.19	102.2	22.6
Benzil	0.11	90.3	23.5	0.11	90.6	23.5

	1b		**1c**	
	T_m/°C	ΔH_m/kJ mol^{-1}	T_m/°C	ΔH_m/kJ mol^{-1}
	150.4	24.2	150.6	24.8

[a] The estimated errors of the DSC measurements are ±0.1 °C for temperatures and ±1% for energies.

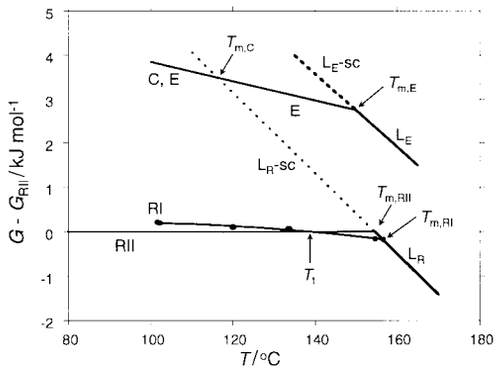

Fig. 8 Stability relationship between the different crystal forms of tazofelone. RI, **1a** (form **I**); RII, **1a** (form **II**); E, enantiomorph (**1b** or **1c**); C, conglomerate; L_R, racemic liquid; L_E, homochiral liquid (+) or (−); L-sc, supercooled liquid. The stability of each form is measured against racemate **II**.

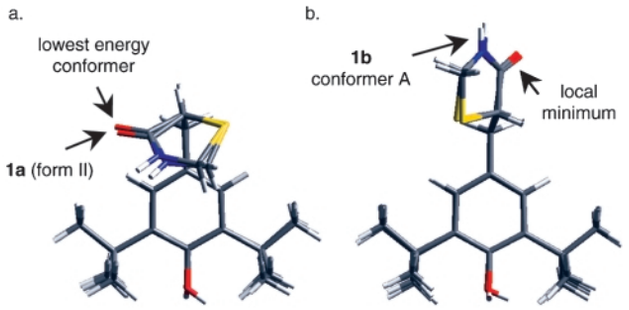

Fig. 9 a) Lowest energy (from conformational search) and form **II** conformers and b) local conformational minimum and conformer A of the enantiomorph. The C–H hydrogen atoms have been omitted for clarity. Note the different relative orientations of the hydroxy group between the observed and calculated structures.

relationship between **I** and **II** is evident from the crossing of the ΔG *vs.* T curve with $\Delta G = 0$ at 138 °C. These data correlate well with the relative solubility of the polymorphic racemic compounds and observed solid-state conversions, which have shown that form **II** (lower melting) is indeed more stable (less soluble) near ambient temperature. Because mixtures of forms **I** and **II** are obtained at crystallization temperatures significantly lower than the transition (crossing) temperature, T_t, the crystallization of **1a** appears to be kinetically-driven.

The entropy and enthalpy differences between forms **I** and **II** were estimated from the slopes of the ΔG *versus* T and $\Delta G/T$ *versus* $1/T$ plots (not shown), respectively: $S_I - S_{II} = 6.8$ J K^{-1} mol^{-1} and $H_I - H_{II} = 2.7$ kJ mol^{-1} (applicable to approximately 60 °C below the melting points). The 2.7 kJ mol^{-1} enthalpy difference, which reflects the lattice energy difference between forms **I** and **II**, is in the expected range for organic polymorphs. In comparison, the free energy difference, ΔG, which is the true measure of relative stability, is considerably smaller (0.2–0.3 kJ mol^{-1}) at the temperatures of measurement. Clearly, the entropy term ($T\Delta S$) contributes significantly to the stability difference between the polymorphs at these temperatures.

Stability relationship between racemic compounds and enantiomorph

The melting data also allow for an evaluation of the stability relationship between the racemic and homochiral crystals (Table 5). Since the enantiomers of **1** do not interconvert, the melts of a racemic compound (R) and an enantiomorph (E) are different. In other words, the racemic mixture of **1** is a two-component system and R and E must be treated as distinct compounds rather than polymorphs.[38] To assess the relative stability of racemic and homochiral crystals, it is necessary to compare R against a one-to-one physical mixture of the opposite enantiomorphs, or a conglomerate (C), which does share the same melt with R. The enthalpy, entropy and free energy differences of R and C are given by the eqns. (5)–(7):

$$(H_R - H_C)(T_{mE}) = \Delta H_{mE} - \Delta H_{mR} + \Delta C_{pR}(T_{mR} - T_{mE}) \quad (5)$$

$$(S_R - S_C)(T_{mE}) = \Delta H_{mE}/T_{mE} - \Delta H_{mR}/T_{mR} + R\ln 2 + \Delta C_{pR}\ln(T_{mR}/T_{mE}) \quad (6)$$

$$(G_R - G_C)(T_{mE}) = \Delta H_{mR}(T_{mE} - T_{mR})/T_{mR} - T_{mE}R\ln 2 + \Delta C_{pR}[T_{mR} - T_{mE} - T_{mE}\ln(T_{mR}/T_{mE})] \quad (7)$$

Here T_{mE} and T_{mR} are the melting points of E and R, respectively; $(H_R - H_C)(T_{mE})$, $(S_R - S_C)(T_{mE})$ and $(G_R - G_C)(T_{mE})$ are, respectively, the enthalpy, entropy, and free energy differences between R and C evaluated at T_{mE}; and ΔC_{pR} is the heat capacity change of R upon melting. Using the melting data in Table 5 and $\Delta C_{pR} = 0.18$ kJ K^{-1} mol^{-1}, which was obtained from the DSC baseline shift upon melting, the thermodynamic parameters of the conglomerate relative to R (form **II**) are estimated as: $H_C - H_{II} = 12$ kJ mol^{-1}, $S_C - S_{II} = 22$ J K^{-1} mol^{-1} and $G_C - G_{II} = 2.8$ kJ mol^{-1}.

The calculated free energies of C, the racemic liquid (L_R) and the liquid of pure enantiomorph (L_E) relative to form **II** (R**II**) are also shown in Fig. 8. The slope of the L_E line is obtained from the entropies of melting of **1b** and **1a** (form **II**). L_E is displaced from L_R by $RT\ln 2$, the mixing entropy of the 1 : 1 mixture relative to the enantiomerically pure liquid.[39] The solidus line of C (and E) was generated using eqns. (6) and (7).

The abundance of racemic compounds (90–95%) relative to conglomerates (5–10%) in crystalline racemates has been taken as evidence that racemic compounds are generally more stable than conglomerates. For individual R–C pairs, the relative thermodynamic stabilities are determined by comparing the melting points of R and C, since these solids are in equilibrium with the same liquid. In the case of **1**, C and R (form **II**) are related monotropically, with form **II** being the higher melting and more stable form at any temperature. Similarly, C was found to be monotropically less stable than R (form **I**).

From the ΔG *vs.* T plot, the temperature at which C would be expected to melt, T_{mC}, is given by the intersection of the supercooled liquid line of R, L_R-sc, with the solid line of C. Note that this temperature (~117 °C) is considerably lower than T_{mE} (150 °C), the melting temperature of pure **1b**. The metastability of C relative to R was confirmed by the DSC trace of a 1 : 1 mixture of **1b** and **1c** crystals (not shown), which featured a very broad, exothermic transition at 80–100 °C, followed by *multiple* high temperature endotherms (150–156 °C). The low temperature transition is presumably due to the partial melting of C and immediate conversion to the racemic compounds (**I**, **II**, or both).

Conformational energies

The observation of significantly different conformers in **1a** and **1b** provides an opportunity to study the influence of crystal forces on molecular conformation and the balance between intra- and intermolecular interactions.[40] One approach to evaluating the influence of crystal forces on molecular conformation is to compare the molecular structure(s) in the solid state with that in the gaseous state,[41] where the minimum energy conformation is expected to predominate. A "global" search for conformational minima was therefore conducted to assess whether the conformations of **1** selected by crystal forces are preferred in the gas phase.[42] The conformational search produced several energetic minima (differing by less than ~2 kcal

Table 6 Conformational energies (kJ mol^{-1}) and dipole moments (debye) of the tazofelone conformers[a]

	1a (I)		1a (II)	1b	
	Conformer A	Conformer B		Conformer A	Conformer B
S1–C5–C6-C7/°	−67.7	67.7	68.6	−62.6	−55.9
C5–C6–C7–C8/°	88.2	−91.0	−88.9	−82.0	132.3
HO^Ph/°	0.167	−0.030	−3.12	−4.45	−0.232
RHF/STO-3G					
ΔE/kJ mol^{-1}	−1.6	2.1	0	6.9	15.9
$\Delta E_{average}$/kJ mol^{-1}	0.3		0	11.4	
Dipole moment/debye	3.48	3.52	3.51	1.81	2.18
RHF/3-21G(*)					
ΔE/kJ mol^{-1}	−2.4	0.3	0	4.1	21.5
$\Delta E_{average}$/kJ mol^{-1}	−1.1		0	12.8	
Dipole moment/debye	4.71	4.77	4.74	2.45	3.11
ΔE(*crystal*)/kJ mol^{-1}	2.7		0	12.1	

[a] Energies, reported relative to the conformer in **1a** (**II**), were calculated by geometry optimization with the non-hydrogen atoms and the HO^Ph angle fixed at crystal positions (see text).

mol^{-1}), which could be candidates for crystal building. The lowest energy conformation, characterized by S1–C5–C6–C7 and C5–C6–C7–C8 torsion angles of 64.6 and −93.2°, respectively, is remarkably similar to that observed in **1a** (forms **I** and **II**), Fig. 9a. The only significant difference is the hydroxy group orientation, which is orthogonal to the phenyl ring in the calculated conformation and coplanar in **1a** (forms **I** and **II**). A higher energy minimum (~4 kJ mol^{-1}) features an extended conformation (S1–C5–C6–C7 = −67.7°, C5–C6–C7–C8 = −82.3°) similar to that observed in conformer A of **1b**, Fig. 9. This conformer also features the hydroxy group oriented perpendicularly to the plane of the phenyl ring.

Conformational energies were calculated for the observed conformers to determine their energies relative to that of the lowest energy conformation and to help rationalize the stability difference between R and C. Single-point energies (RHF/3-21G(*)) calculated using the atom coordinates obtained from the X-ray structures showed the conformers in **1b** and **1c** to be as much as 200 kJ mol^{-1} higher in energy than those in **1a**, energies which are entirely unreasonable for conformers related by single-bond torsions. To determine if the large energy differences were due to the misplacement of hydrogen atoms in the X-ray structures, we conducted geometry optimizations (RHF/STO-3G and RHF/3-21G(*)) in which all non-hydrogen atoms were fixed, as well as the hydroxy orientation relative to the phenyl ring. The conformational energy differences thus obtained (Table 6) were much more reasonable (on the order of 4 kJ mol^{-1}). Optimization of hydrogen atom positions therefore appears to be imperative to performing conformational energy calculations using X-ray coordinates.

The relative energies of the three **1a** conformers (RIA, RIB and R**II**) calculated at the RHF/STO-3G and RHF/3-21G(*) levels are comparable (Table 6), as would be expected from their nearly identical conformations. The **1b** conformers, on the other hand, are substantially higher in energy (*e.g.*, conformer A: +4.0 kJ mol^{-1}, conformer B: +21.5 kJ mol^{-1}). In addition, the **1b** conformers were found to have significantly smaller dipole moments than the **1a** conformers. The adoption of high-energy and low-dipole conformations, which likely contribute to the higher lattice energy of **1b**, must be a result of the geometry requirement for the formation of intermolecular hydrogen bonds. Minimally, hydrogen-bonding interactions are responsible for the coplanarity of the hydroxy group and the phenyl ring in all of the crystal forms of **1**.

Lattice energy calculations

From the conformational analysis, the *intramolecular* contributions to the stability of the crystal forms of **1** could be evaluated. Since the total energy of a system is the sum of the intramolecular (*i.e.* conformational) and intermolecular (*i.e.* lattice energy) contributions,[41] lattice energy calculations were also performed in an attempt to assess the stability differences between **1a** (forms **I** and **II**) and **1b** in terms of *intermolecular* interactions. The calculated differences in lattice energy relative to form **II**, as well as the contributions of electrostatic forces, van der Waals forces, and hydrogen bonds (differentiated by the DREIDING force field only), are given in Table 7.

The calculated lattice energies of **1a** (forms **I** and **II**) and **1b** are significantly different from the enthalpy differences determined calorimetrically (Table 5).[43] Given the limited accuracy of the force fields used in crystal modeling, it is not surprising that the small energy difference (2.7 kJ mol^{-1}) of forms **I** and **II** could not be predicted. It is reassuring, however, that the significantly higher energy of **1b** was computationally reproduced, although the calculated energy difference (238–280 kJ mol^{-1}) was some 20 times greater than the experimental value. These results possibly reflect the inadequacy of the force field approach and the use of atomic charges obtained from room temperature structures as input to crystal modeling at 0 K. The force field inadequacy in the case of tazofelone is evidenced by a significant distortion of the enantiomorph unit cell and hydrogen-bonding pattern observed using the CFF and CVFF force fields.

Discussion

Three principles of crystal packing, specifically enumerated to account for space group frequencies, have been shown to govern crystal stability: (1) maximize density (minimize free volume), (2) satisfy intermolecular interactions (*e.g.*, H-bond donor and acceptor sites), and (3) minimize electrostatic energy. In the racemic and chiral crystals of tazofelone, molecular conformation must also be considered because the molecule can change conformation in response to different hydrogen bonding and/or crystal packing requirements. Here, we examine the factors, which collectively describe the crystal lattice energies of tazofelone: conformational energy, hydrogen bonding, and van der Waals and dipole–dipole interactions:[44]

$$E_{\text{lattice}} = E_{\text{conformational}} + E_{\text{hydrogen bonding}} + E_{\text{van der Waal's}} + E_{\text{electrostatic}}$$

Table 7 Calculated lattice energies of tazofelone racemates and enantiomorph (kJ mol^{-1})[a]

	1a (I)	1a (II)	1b
DREIDING force field			
$\Delta E_{lattice}$/kJ mol^{-1}	−7.9	0	282.0
a/Å	11.306 (0.1)	17.430 (1.3)	9.423 (0.3)
b/Å	17.169 (0.5)	11.357 (0.6)	11.131 (1.6)
c/Å	19.712 (2.0)	19.147 (1.5)	17.749 (0.4)
β/°	103.44 (2.3)	—	93.72 (0.6)
ΔE_{VDW}/kJ mol^{-1}	−4.2	0	15.9
ΔE_{elec}/kJ mol^{-1}	−5.9	0	277.0
ΔE_{HB}/kJ mol^{-1}	−0.4	0	7.1
CVFF force field			
$\Delta E_{lattice}$/kJ mol^{-1}	−9.2	0	262.3[b]
a/Å	11.171	16.882	9.262
b/Å	16.880	11.278	11.415
c/Å	19.481	19.538	11.896
β/°	102.76	—	90.50
CFF force field			
$\Delta E_{lattice}$/kJ mol^{-1}	−2.5	0	240.2[b]
a/Å	11.183	17.250	9.259
b/Å	16.964	11.203	11.370
c/Å	19.304	18.319	16.987
β/°	104.61	—	95.97

[a] Energies are reported relative to **1a** (**II**). Numbers in parentheses are the percentage change from the unit cell parameters observed crystallographically. [b] A major crystal structural change was observed, resulting in a different hydrogen-bonding pattern.

Conformational preferences

Although bond lengths and angles do not change significantly between polymorphs, single-bond torsion angles are often different because torsional energies can be readily overcome by crystal forces (conformational polymorphism). In **1a** (forms **I** and **II**), each enantiomer adopts its lowest energy conformation, which is further stabilized by efficient hydrogen bonding (amide dimer) and crystal packing. Since a similar amide dimer cannot form between conformers of the same chirality due to significant steric interactions, **1b** adopts high energy (+4 and +20 kJ mol^{-1}), low-dipole conformers that can be stabilized by different, but efficient, hydrogen bonding and crystal packing. Although a variety of intermolecular forces may stabilize conformer A (+4 kJ mol^{-1}), hydrogen-bonding interactions are most likely needed to stabilize conformer B (+20 kJ mol^{-1}). The less stable conformers clearly contribute to the higher crystal lattice energy of **1b**.[45,46]

Hydrogen-bonding interactions

The hydrogen-bonding preferences of the tazofelone donors and acceptors must be satisfied for the molecular conformations adopted in **1a** (forms **I** and **II**) and **1b**. Hydrogen-bonding rules, formulated for organic structures to reflect energetically favorable kinds of intermolecular interactions, state that all good donors[47] and acceptors[48] will participate in hydrogen bonding. As shown by X-ray crystallography and solid-state spectroscopy, the hydrogen-bonding interactions identified in **1a** (forms **I** and **II**) and **1b** are completely different, yet all donors (NH and OH) and good acceptors (amide C=O) participate in hydrogen bonding in each structure.

For crystals of molecules containing multiple donors and acceptors, another useful rule for predicting stable hydrogen-bonded aggregates states that the best donor will hydrogen bond to the best acceptor.[49] In **1a** (forms **I** and **II**), the best donor (amide NH) is hydrogen-bonded to the best acceptor (amide C=O) to form an amide dimer, the most commonly observed aggregate formed by primary amides and lactams.[50] The amide dimer is disrupted in **1b**, however, as a heterodimer is formed between the amide and phenol OH. This unusual hydrogen-bonding pattern, which has not been observed in any structures containing lactams and phenols retrieved from the Cambridge Crystallographic Database, is presumably less stable.

van der Waals interactions

The cohesive energy of many comparatively weak van der Waals interactions can contribute as much as 40–100 kJ mol^{-1} to crystal lattice energies. Thus, while crystal packing is often dictated by hydrogen-bonding interactions when three-dimensional networks result, the packing of one or two-dimensional hydrogen-bonded aggregates is usually controlled by van der Waals interactions.[51] This appears to be the case in the crystal structures of **1**, where three hydrogen-bonding interactions link molecules in two-dimensional layers in **1a** (forms **I** and **II**) and one-dimensional chains in **1b**.

Crystals which are controlled by van der Waals interactions are characterized by close packing. In accordance with Kitaigorodsky's Close-Packing Principle,[52] which states that the most stable form should have the highest packing coefficient (or density), the racemate structures might be expected to be more efficiently packed, *i.e.*, more dense, than the enantiomeric form.[53] Contrary to the Close-Packing Principle and also to Wallach's rule,[54] which states that racemic compounds tend to be more dense than their chiral counterparts, **1a** (forms **I** and **II**) and **1b** have comparable packing efficiencies and densities.[55] Thus, the stability relationships between these crystal forms are not likely due to significant differences in the van der Waals contributions to the crystal lattice energy.

Dipole–dipole interactions

Dipole–dipole interactions contribute to the overall electrostatic energy in molecular crystals, a contribution which has been shown to be negligible for some small-molecule systems,[56] but which is large relative to the energies of van der Waals interactions. While the electrostatic contribution to the lattice energy of a molecular crystal is not a determining factor for crystal packing, its effect on the crystal lattice energy is not always negligible. The molecular dipole moments of the conformers in **1a** (forms **I** and **II**) are significantly larger than those in **1b** (Table 6). Although a previous study has shown that there is no correlation between the magnitude of the molecular

dipole moment and relative orientations of molecules in the solid state,[57] it is interesting to note that in the crystal structures of **1**, the conformer with the largest dipole moment crystallizes in two centrosymmetric space groups and the conformations with the smaller dipole moments pack in a noncentrosymmetric structure. Thus, while the relative importance of dipole–dipole interactions is arguably small, these presumably weaker electrostatic interactions in **1b** possibly contribute to its higher lattice energy.

Conclusions

Tazofelone has been isolated and characterized in two racemic polymorphs, **1a** (forms **I** and **II**), and as an enantiomorph, **1b**. Forms **I** and **II** are structurally very similar, both exhibiting topologically identical two-dimensional hydrogen-bonded layers. The main structural difference occurs in the packing of these layers in the third dimension. Forms **I** and **II** are enantiotropically related, with **II** being more stable than **I** below the transition temperature of 138 °C. The ease with which mixtures of these polymorphic forms are obtained may be explained in terms of their small free energy difference, which may be readily overcome by kinetic factors during crystallization.

The solid-state structures adopted by **1** result from the delicate balance between intramolecular and intermolecular forces. The molecular conformation, hydrogen-bonding, and crystal packing observed in **1a** (forms **I** and **II**) are significantly different from **1b**. Tazofelone adopts a high energy conformation in **1b**, which enables all hydrogen-bond donors and good acceptors to be used and allows for efficient crystal packing. As a result of its considerably higher conformational energies and somewhat less stable hydrogen-bonding pattern, the conglomerate is monotropically less stable than either racemic compound. Thus, a spontaneous resolution of a racemic solution is not feasible thermodynamically at any temperature.

Acknowledgements

The authors wish to thank Jennifer Wilkie and Greg Stephenson for crystallographic assistance.

References

1 C. Aakeröy, *Acta Crystallogr.*, *Sect. B*, 1997, **53**, 569.
2 J. Bernstein, Conformational Polymorphism, in *Organic Solid State Chemistry*, ed. G. R. Desiraju, Elsevier, Amsterdam, 1987.
3 C. Aakeröy, A. M. Beatty, M. Nieuwenhuyzen and M. Zou, *J. Mater. Chem.*, 1998, **8(6)**, 1385.
4 J. Jacques, A. Collet and S. H. Wilen, *Enantiomers, Racemates and Resolutions*, John Wiley & Sons, New York, 1981.
5 W. C. McCrone, *Physics and Chemistry of the Organic Solid State*, eds. D. Fox, M. M. Labes and A. Weissberger, Interscience, New York, 1965, vol. 2, p. 725.
6 D. E. Drayer, *Clin. Pharmacol. Ther.*, 1986, **40**, 125.
7 Z. J. Li and D. J. W. Grant, *J. Pharm. Sci.*, 1997, **86**, 1073; T. R. Kommuru, M. A. Khan and I. K. Reddy, *J. Pharm. Sci.*, 1998, **87**, 833.
8 R. L. Smith and J. Caldwell, *Trends Pharmacol. Sci.*, 1988, **9**, 75; W. H. De Camp, *Chirality*, 1989, **1**, 2.
9 J. A. Panetta, J. K. Shadle, M. L. Phillips, D. N. Benslay and P. P. K. Ho, *Ann. N. Y. Acad. Sci.*, 1993, **696**, 415.
10 M. L. Phillips, D. M. Berry and J. A. Panetta, *J. Org. Chem.*, 1992, **57**, 4047.
11 A. R. Harkness and M. M. Hansen, unpublished work.
12 M. L. Phillips and J. A. Panetta, *Tetrahedron: Asymmetry*, 1997, **8(13)**, 2109.
13 S. Hayashi and K. Hayamizu, *Bull. Chem. Soc. Jpn.*, 1991, **64**, 688.
14 G. M. Sheldrick, *SHELXTL-PLUS*, Program for Siemens R3m/V crystallographic systems, Version 4.1, Siemens Crystallographic Research Systems, New Jersey, 1990.
15 G. M. Sheldrick, SHELXL-86. Program for the Solution of Crystal Structures, University of Cambridge, 1986.
16 G. M. Sheldrick, SHELXL-93. Program for Crystal Structure Determination, University of Göttingen, 1993.
17 Cerius² Molecular Modeling Software, Version 3.6, BIOSYM/Molecular Simulations, Inc.
18 Cambridge Structural Database; Cambridge Crystallographic Data Centre, 12 Union Road Cambridge, CB2 1EZ, United Kingdom, Version 5.14, October 1997.
19 Spartan Version 5.0, Wavefunction, Inc., Irvine, CA, USA.
20 S. L. Mayo, B. D. Olafson and W. A. Goddard III, *J. Phys. Chem.*, 1990, **94**, 8897.
21 J. R. Maple, U. Dinar and A. T. Hagler, *Proc. Natl. Acad. Sci. USA*, 1988, **85**, 5350.
22 P. Dauber-Osguthorpe, V. A. Roberts, D. J. Osguthorpe, J. Wolff, M. Genest and M. T. Hagler, *Proteins: Struct.*, *Funct.*, *Genet.*, 1988, **4**, 31.
23 M. C. Etter, *Acc. Chem. Res.*, 1990, **23**, 120; M. C. Etter, J. C. MacDonald and J. Bernstein, *Acta Crystallogr.*, *Sect. B*, 1990, **46**, 256.
24 S. C. Nyburg and C. H. Faerman, *Acta Crystallogr.*, *Sect. B*, 1985, **41**, 274.
25 C. B. Aakeröy and K. R. Seddon, *Chem. Soc. Rev.*, 1993, 397; *The Hydrogen Bond. Recent Developments in Theory and Experiments Vols. I-III*, eds. P. Schuster, G. Zundel and C. Sandorfy, North Holland, Amsterdam, 1976; R. Taylor and O. Kennard, *Acc. Chem. Res.*, 1984, **17**, 320; R. Taylor and O. Kennard, *J. Am. Chem. Soc.*, 1982, **104**, 5063.
26 JOWTIY = 1-ethyl-3-((3′,5′-di-*tert*-butyl-4′-hydroxyphenyl)methylene)-5-(2′-carboxybenzyloxy)-2-oxindole, J. J. Valentine, S. Nakanishi, D. L. Hageman, R. M. Snider, R. W. Spencer and F. J. Vinick, *Bioorg. Med. Chem. Lett.*, 1992, **2**, 333. VOGMAF = (*E*)-*N*-(4,6-dimethylpyridin-2-yl)-3-(3,5-di-*tert*-butyl-4-hydroxyphenyl)-pyrrolidin-2-one, N. Rodier, J. M. Robert, S. Robert-Piessard and G. Le Baut, *Acta Crystallogr.*, *Sect C*, 1991, **47**, 2684.
27 The packing coefficient, κ, represents the amount of space filled by molecules in a lattice and is calculated as $N(V_{vdw}/V_{cell})$, where N is the number of molecules in the unit cell, V_{vdw} is the van der Waals volume of the molecule and V_{cell} is the volume of the unit cell. The van der Waals volumes were calculated using the Connolly surface feature (probe radius = 0) of the Cerius² program and the standard van der Waals radii of the program.
28 A. I. Kitaigorodsky, *Molecular Crystals and Molecules*, Academic Press: New York and London, 1973.
29 C. P. Brock and J. D. Dunitz, *Chem. Mater.*, 1994, **6**, 1118.
30 H. G. Brittain, *J. Pharm. Sci.*, 1997, **86**, 405.
31 J. G. Hexem, M. H. Frey and S. J. Opella, *J. Chem. Phys.*, 1982, **77**, 3847; J. G. Hexem, M. H. Frey and S. J. Opella, *J. Am. Chem. Soc.*, 1981, **103**, 224; A. C. Olivieri, L. Frydman and L. E. Diaz, *J. Magn. Reson.*, 1987, **75**, 50.
32 S. J. Opella and M. H. Frey, *J. Am. Chem. Soc.*, 1979, **101**, 5854.
33 A. Naito, S. Tuzi and H. Saito, *Eur. J. Biochem.*, 1994, **224**, 729.
34 A. Burger and R. Ramberger, *Mikrochim. Acta [Wien] II*, 1979, 259.
35 The relevant equations for calculating the ΔG between true polymorphs using pure melting data have been previously described. L. Yu, *J. Pharm. Sci.*, 1995, **84**, 966.
36 The use of a series of eutectic melting points to characterize organic crystals has been described by McCrone. W. C. McCrone, *Fusion Methods in Chemical Microscopy*, Interscience Publishers, Inc., New York, 1957; This technique has been extended to using DSC for the quantitative determination of ΔG. L. Yu, G. A. Stephenson, C. A. Mitchell, C. A. Bunnell, S. V. Snorek, J. J. Bowyer, T. B. Borchardt, J. G. Stowell and S. R. Byrn, *J. Am. Chem. Soc.*, 2000, **122**, 585 (web posting 1/19/2000).
37 More rigorous forms of eqns. (1)–(4) contain additional terms: heat capacity terms [eqns. (1)–(4)] and concentration-dependent terms [eqns. (3)–(4)]. All are negligible for tazofelone racemates **I** and **II**.
38 Racemates and enantiomorphs are considered to be polymorphic when the interconversion of enantiomers in the melt is fast. J. D. Dunitz, *Acta Crystallogr.*, *Sect. B*, 1995, **51**, 619.
39 For similar packing energies, racemates tend to melt at lower temperatures than their chiral counterparts because the racemic liquid has a higher entropy (of mixing) and thus, a lower free energy.
40 J. Bernstein, *J. Phys. D: Appl. Phys.*, 1993, **26**, B66.
41 D. Buttar, M. H. Charlton, R. Docherty and J. Starbuck, *J. Chem. Soc.*, *Perkin Trans. 2*, 1998, 763.
42 Given that *ab initio*, HF calculations are quite time-consuming, the search of conformational space was restricted to geometry optimizations of conformers produced by systematically varying the two torsion angles which describe the molecular shape in form **II** in 120° jumps (3 × 3 matrix). The lowest energy conformation in this relatively crude search of conformational space may not necessarily be the global energy minimum.
43 Force fields have previously been shown to adequately predict similar energies of polymorphs, but not necessarily their stability

order. See: J. C. Osborn and P. York, *AAPS Annual Meeting Abstracts*, 1997, **14**, p. S188.
44 $E_{electrostatic}$ includes contributions from dipole–dipole interactions.
45 G. R. Desiraju, *Organic Solid State Chemistry*, Elsevier, Amsterdam, 1987.
46 The high energy conformers also contribute to the low eutectic melting temperature of the conglomerate (T_{mC}) and the entropy difference, $S_C - S_{II}$ (22 J K^{-1} mol^{-1}). Thermal motion and/or disorder of the five-membered ring of one of the **1b** conformers (identified by the comparatively large thermal ellipsoids in Fig. 2) may be another source of the substantial entropy difference.
47 J. Donahue, *J. Phys. Chem.*, 1952, **56**, 502.
48 M. C. Etter, *J. Phys. Chem.*, 1991, **95**, 4601.
49 M. C. Etter, *Acc. Chem. Res.*, 1990, **23**, 120.
50 L. Leiserowitz and M. Tuval, *Acta Crystallogr.*, *Sect. B*, 1978, **34**, 1230.
51 Lattice energy differences in the 4–8 kJ mol^{-1} range are expected for polymorphic organic crystals dominated by van der Waals interactions. See A. I. Kitaigorodsky, *Adv. Struct. Res. Diffr. Methods*, 1970, **3**, 173.
52 A. Kitaigorodsky, *Organic Chemical Crystallography*, Consultant's Bureau: New York, 1961; *trans*-1,2-Dibromoacenaphthene and resorcinol are other exceptions to the close-packing rule. See G. Nonnenmacher and R. Mecke, *Z. Anal. Chem.*, 1959, **170**, 127.
53 Strong, directional hydrogen-bonding interactions sometimes work in opposition to the Close-Packing Principle, resulting in stable, but less efficiently packed, molecular crystals.
54 O. Wallach, *Liebigs Ann. Chem.*, 1895, **286**, 90.
55 The validity of Wallach's rule has previously been challenged, as no clear correlation was found to exist between racemate/enantiomer formation and crystal density using unbiased samples. See C. P. Brock, W. B. Schweizer and J. D. Dunitz, *J. Am. Chem. Soc.*, 1991, **113**, 9811.
56 A. Gavezotti, *J. Phys. Chem.*, 1990, **94**, 4319.
57 J. K. Whitesell, R. E. Davis, L. L. Saunders, R. J. Wilson and J. P. Feagins, *J. Am. Chem. Soc.*, 1991, **113**, 3267.